IOPscience iopscience.iop.org

Home Search Collections Journals About Contact us My IOPscience

Proposal of a broadband, polarization-insensitive and high-efficiency hot-carrier schottky photodetector integrated with a plasmonic silicon ridge waveguide

This content has been downloaded from IOPscience. Please scroll down to see the full text.

2015 J. Opt. 17 125010

(http://iopscience.iop.org/2040-8986/17/12/125010)

View the table of contents for this issue, or go to the journal homepage for more

Download details:

IP Address: 61.164.42.140
This content was downloaded on 31/03/2016 at 08:08

Please note that terms and conditions apply.

IOP Publishing Journal of Optics

J. Opt. 17 (2015) 125010 (10pp) doi:10.1088/2040-8978/17/12/125010

Proposal of a broadband, polarization-insensitive and high-efficiency hot-carrier schottky photodetector integrated with a plasmonic silicon ridge waveguide

Liu Yang[1,2], Pengfei Kou[1], Jianqi Shen[1], El Hang Lee[1] and Sailing He[1,3]

[1] Centre for Optical and Electromagnetic Research, Zhejiang Provincial Key Laboratory for Sensing Technologies, State Key Laboratory of Modern Optical Instrumentation, Department of Optical Engineering, Zhejiang University, Hangzhou 310058, People's Republic of China
[2] School of Electrical, Computer, and Engineering, Arizona State University, Tempe, AZ 85287, USA
[3] Department of Electromagnetic Engineering, JORCEP [Joint Research Center of Photonics of Zhejiang University and KTH], Royal Institute of Techtnology (KTH), S-100 44 Stockholm, Sweden

E-mail: optyang@zju.edu.cn and sailing@jorcep.org

Received 31 May 2015, revised 29 September 2015
Accepted for publication 30 September 2015
Published 5 November 2015

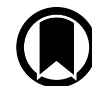

Abstract

We propose a broadband, polarization-insensitive and high-efficiency plasmonic Schottky diode for detection of sub-bandgap photons in the optical communication wavelength range through internal photoemission (IPE). The distinctive features of this design are that it has a gold film covering both the top and the sidewalls of a dielectric silicon ridge waveguide with the Schottky contact formed at the gold–silicon interface and the sidewall coverage of gold can be easily tuned by an insulating layer. An extensive physical model on IPE of hot carriers is presented in detail and is applied to calculate and examine the performance of this detector. In comparison with a diode having only the top gold contact, the polarization sensitivity of the responsivity is greatly minimized in our photodetector with gold film covering both the top and the sidewall. Much higher responsivities for both polarizations are also achieved over a broad wavelength range of 1.2–1.6 μm. Moreover, the Schottky contact is only 4 μm long, leading to a very small dark current. Our design is very promising for practical applications in high-density silicon photonic integration.

Keywords: silicon, photodetectors, surface plasmons

(Some figures may appear in colour only in the online journal)

1. Introduction

Internal photoemission (IPE) is an intrinsic property of a Schottky diode, occurring at a metal–semiconductor interface [1]. In IPE, three processes are involved. Firstly, an electron (hole) in the metal is excited to a higher level after absorbing a photon, becoming a hot electron (hot hole). Secondly, the hot carrier (electron or hole) travels to the metal–semiconductor interface. During its travel, the hot carrier may lose some energy due to scattering by cold carriers or to thermal relaxation. Finally, upon arrival at the interface, it can cross over the Schottky barrier into the semiconductor if its remaining energy is still higher than the barrier. All the emitted hot carriers in the semiconductor will then be quickly swept away in the form of photocurrent and will be collected by the Ohmic contact electrode. As long as the photons have higher energies than the Schottky barrier (not necessarily higher than the bandgap of the compositional semiconductor), they can be converted to current. Therefore, the IPE mechanism is often used to determine the Schottky barrier height of a metal–semiconductor interface [1]. In recent years, IPE has been explored as one of the most attractive means to

 © 2015 IOP Publishing Ltd Printed in the UK

realize detection of photons below the semiconductor bandgap for sensing [2–4], solar energy conversion [5–7], and optoelectronic devices for optical communication [8–14].

In particular, for planar silicon (Si)-based photodetectors, sub-bandgap photons in the optical communication wavelength range of 1.2–1.6 μm, can be readily detected based on the IPE mechanism, since a metal (or silicide)-Si based Schottky diode usually has a much lower Schottky barrier than the Si bandgap energy (1.1 eV) [8–14]. This method is much simpler in comparison with previously reported methods, such as hybrid integration of low-bandgap semiconductors [15], creating defect-induced levels in the bandgap (which may cause high dark current) [16, 17], or employing the two-photon absorption effect (which requires high input power or high Q-factor cavities) [18]. However, the IPE probability of a Si-based Schottky diode, determined by the Schottky barrier, metal thickness, and the input photon energy, is not very high, thereby leading to low internal quantum efficiency (IQE) and hence low responsivity [19]. Fortunately, it can be improved by properly choosing a metal (or silicide)–Si pair having a low Schottky barrier [8–10]. Another effective way of improving the responsivity is to increase the metallic absorption as much as possible so as to increase the external quantum efficiency of the Schottky device with a certain IPE probability. Plasmonic waveguides in the form of asymmetric [11] and symmetric [12] gold (Au) strips, or Au-capped photonic bus waveguide [13], have been proposed to form Schottky photodetectors, where the light waves propagating along the Au–Si interface can be highly absorbed in the metal. The absorption in the active silicide layers can also be greatly improved by inserting a silicide Schottky diode in a metallic slot and forming a metal–insulator–silicon–insulator–metal nanoplasmonic slot waveguide [10]. However, these plasmonic photodetectors [10–13] all respond more strongly to one of the orthogonal polarizations than the other due to the intrinsic polarization sensitivity of plasmonic strip or slot waveguides [20]. And thus, they are not suitable for practical applications such as optical interconnect system, which requires polarization insensitivity. Moreover, light waves are not so well confined in these plasmonic strip waveguides, thus requiring the photodetectors to be long (tens of micrometers) [11–13] and thereby significantly limiting the integration density. The dark current, which is proportional to the metal–semiconductor contact area, is also very high in these structures. For the silicide Schottky diode based on the nanoplasmonic slot waveguide [10], unlike those reported in [11–13], the unavoidable large loss in metal (not the active material) can be detrimental to the overall performance.

In order to overcome these shortfalls, we propose in this paper a new Schottky diode design based on a metal-coated Si ridge waveguide. It has a Au film covering both the top and the sidewalls of a dielectric silicon ridge waveguide with the Schottky contact formed at the Au–Si interface. This design is similar to the one published in [14], where the authors did not investigate the polarization property or its tunability. Here, we use a SU8 insulator layer on the Si slab of the ridge waveguide to make the device to respond almost equivalently to both transverse-electric (TE) and transverse-magnetic (TM) polarized light by simply varying the insulator thickness. We have analyzed and investigated the characteristics of our Schottky photodiode in more detail in terms of the polarization property or its tunability, which was lacking in other studies like [14]. Here, to simulate our device, the physical model in [19], which cannot be applied directly, is extended and presented in detail. Our results show that the new diode is not only polarization-insensitive but also highly absorptive. Over 85% of light in the broad wavelength range of 1.2–1.6 μm can be absorbed within the Schottky diode of only 4 μm in length. We have found that our photodetector shows greatly improved performance in comparison with the one without sidewall coverage of Au as reported in [13]. For the emerging graphene material, photocurrent can also be observed from the IPE effect [21, 22]. However, this is not the only reason for the measured photocurrent, to which the excitation of the intrinsic graphene electrons also contribute [21]. Here in our design, Si cannot generate any free carriers under the illumination of the light in the optical communication wavelength range. The IPE effect is the only mechanism for the generation of photocurrent, and this is different from that for the graphene-antenna photodetector [21]. In addition, broadband and polarization-insensitive optoelectrical responses can be easily achieved for our Schottky diode based on the plasmonic waveguide, but are difficult to be realized by the resonant antenna dominated graphene photodetector [20].

2. Structure and physical model

The schematic structure of our proposed photodetector is shown in figure 1(a). It consists of a Si ridge waveguide, an Au Schottky electrode (of thickness, h_{Au}) covering both the top and the sidewalls of the Si ridge, an aluminium (Al) Ohmic electrode on the top of the Si slab, and a thin SU8 insulating film (of thickness, h_{SU8}) separating the two electrodes. The distinctive features, different from any of the previously reported structures [8–13], are the Au-covered Si ridge waveguide, which forms a special plasmonic waveguide, and the tunability of the Au coverage by the SU8 insulating layer. The Schottky contact is formed at the Au–Si interface, as shown in figure 1(b). With the sidewall coverage of Au, not only the quasi-TE mode with dominant x-component of the electric field but also the quasi-TM mode with dominant y-component of the electric field (which will be shown later) can be excited, and the absorption can be achieved for both polarizations. The input Si ridge waveguide is designed as a single-mode dielectric waveguide with typical structural parameters of ridge width $w_{\mathrm{r}} = 350$ nm, ridge height $h_{\mathrm{r}} = 250$ nm, and slab thickness $h_{\mathrm{sl}} = 50$ nm. Sub-bandgap photons guided along the Si ridge waveguide are directly coupled to the connected plasmonic waveguide, where they are absorbed by the Au electrode and converted into photocurrent through the IPE effect. For comparison, we also considered the case when $h_{\mathrm{SU8}} = 200$ nm, as shown in figure 1(c), which is similar to the Au-capped waveguide

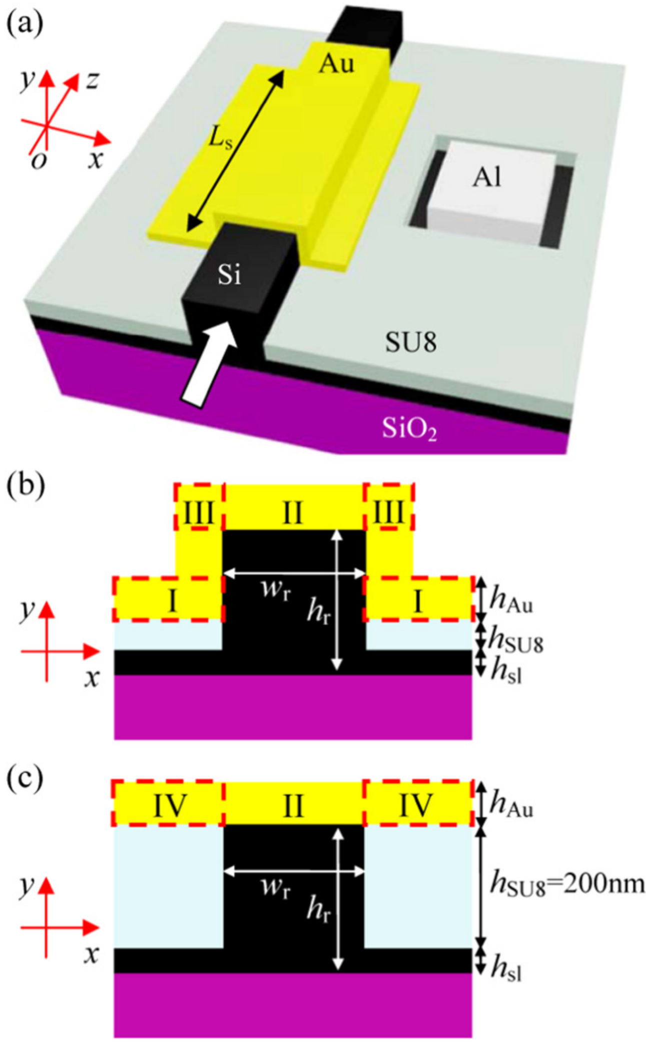

Figure 1. (a) Three-dimensional schematic diagram of our Si photodetector. Two-dimensional cross-sectional schematic diagrams with (b) $h_{SU8} < 200$ nm and (c) $h_{SU8} = 200$ nm.

detector reported in [13]. The other structural parameters are kept the same for the sake of comparison.

Generally, the responsivity, R, of a photodiode in the short-circuit operation mode can be obtained from its IQE as follows:

$$R = \frac{q}{h\nu} \cdot A \cdot \text{IQE}, \tag{1}$$

where A is the light absorption, q is the elemental charge, h is the Planck's constant, and ν is the frequency of the incident photon. This physical parameter, R, measures the electrical current output per optical input power in unit of mA W^{-1} and is a main figure of merit for us to optimize our Schottky diode and analyze its polarization sensitivity. In our IPE-based Schottky diode, the IQE, which means how many hot carriers being excited can jump over the Schottky barrier into the Si ridge waveguide, is dependent on the emission probability, $P(E)$, of the hot carriers and can be obtained by integrating all the emission probabilities in the energy range from the Schottky barrier height, Φ_B, to the initial excess energy above the Fermi level, E_0, expressed as follows:

$$\text{IQE} = \frac{1}{E_0}\int_{\Phi_B}^{E_0} P(E)\,\mathrm{d}E. \tag{2}$$

$P(E)$ is a very important parameter for estimating IQE. Before deriving $P(E)$, two assumptions are made: (i) hot carriers which do not emit through the Au–Si interface will be reflected elastically; and (ii) those traveling to the Au–air or Au–SU8 interface cannot transmit through it but instead are totally and elastically reflected back. Then, according to these assumptions, only hot carriers traveling in the direction along the normal of the Au–Si interface have an opportunity for emission. For our detector shown in figure 1(b), the Au–Si interfaces in regions I and II can be regarded to be flat and $P(E)$ can be calculated by equations (3.1) and (3.2) according to the number of round trips the hot carriers can travel in the Au film, which have been derived in [19].

$$P(E) = P_{\rm i} = \frac{1}{2}(1 - \cos\Omega), \quad \text{when } N = 0; \tag{3.1}$$

$$P(E) = P_{\rm ii} = P_0 + (1 - P_0)P_1 + (1 - P_0)(1 - P_1)P_2 + \cdots + P_N \prod_{m=0}^{N-1}(1 - P_m), \ \text{when } N > 0, \tag{3.2}$$

where Ω is the solid angle determined by $k \cdot \cos\Omega = k_{SB}$, leading to $\cos\Omega = \sqrt{\Phi_B/E}$ as shown in figures 2(a) and (b); $P_{x(0-N)} = P(E_x) = \frac{1}{2}\left(1 - \sqrt{\frac{\Phi_B}{E_x}}\right)$ is the emission probability of a hot carrier whose energy is reduced from E_0 to $E_x = E_0 e^{-2xh_{Au}/L}$ after traveling an x-number of round trips within the Au film. $N = \frac{L}{2h_{Au}}\ln\left(\frac{E_0}{\Phi_B}\right)$ is an integer, representing how many round trips a hot carrier can travel back and forth within the Au film before its energy E_0 is reduced to Φ_B and it has no chance to jump over the Schottky barrier; L is the mean free path of 74 nm (55 nm) for an electron (a hole) in Au [23]. For a given Au–Si Schottky contact, $\Phi_B = 0.34$ and 0.8 eV are chosen from the measurement results reported in [1] as the only physical parameter to characterize the interfacial property of Au-p-Si and Au-n-Si interfaces, respectively. Here, the Si is lightly doped with dopant density in the order of 10^{14}–10^{16} cm^{-3}. Since Φ_B depends only weakly on the doping density through the image force barrier lowering, such effect can be neglected, especially under zero bias considered in this work. As reported in the review article [24], surface states induced by the interfacial defects or the chemical bonding between the metal and the semiconductor play an important role in influencing Φ_B. If the surface state density is very low, Φ_B is mainly determined by the metal work function and the semiconductor electron affinity. Otherwise, the Fermi level will be pinned at the value above the valence band and Φ_B will then be mainly determined by the surface properties of the semiconductor [25]. By using the measured values of Φ_B mentioned above, which have already considered the effects of the doping density and the surface states in real devices, the physical model can be simplified [11, 12, 19]. In this case, we can focus on the main effect of

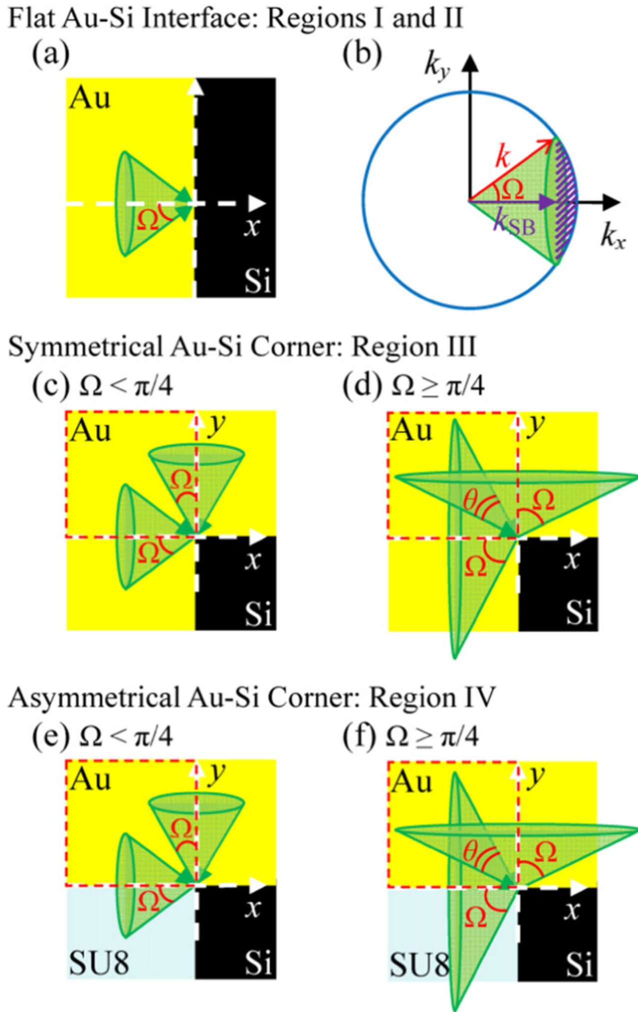

Figure 2. Emission cones with angle Ω: (a) a real-space and (b) a momentum–space illustrations for flat Au–Si interfaces; (c)–(f) real-space illustrations for (c),(d) a symmetrical Au–Si corner and (e),(f) an asymmetrical corner denoted by red dashed rectangles when (c), (e) $\Omega < \pi/4$ and (d),(f) $\Omega \geqslant \pi/4$.

the thin Au film on the IPE probability and consequently the optical responses as a result of its coverage on the Si ridge waveguide. Therefore, N is determined by the photon energy E_0 and the Au film thickness h_{Au}. If E_0 (photon wavelength, λ) becomes larger (smaller) and h_{Au} becomes thinner, the hot carriers will undergo more round trips in the Au film (i.e. $N > 0$), leading to higher $P(E)$. This thus results in higher IQE according to equation (2) and is clearly demonstrated in figure 3(a) for the p-Si based Schottky contact. When h_{Au} gets sufficiently thick, N will be reduced to zero and as a result $P(E)$ and IQE become independent of h_{Au}. In this case, $P(E) = P_{\mathrm{ii}}$ is reduced to P_{i}. The black dotted curve in figure 3(a) shows where N becomes zero. It shows that $h_{\mathrm{Au}}|_{N=0}$ becomes thinner as λ increases (or E_0 decreases). For n-Si based Schottky contact, IQE is about one order of magnitude smaller than that for the p-Si based Schottky contact as shown in figure 3(b) and is independent of h_{Au} in the whole wavelength range considered here. This is mainly due to the high Φ_{B} which prevents hot carriers excited by photons in this range to travel a complete round trip in the Au film even when its thickness is as small as 10 nm. In region I, the Au slab is thick enough horizontally and is much larger than the thicknesses denoted by the black dotted line in figure 3(a) for the Au-p-Si interface. Thus, $P(E)$ in this region is basically equal to P_{i} in equation (3.1). For the Au film in region II, h_{Au} is not as thick as that in region I and becomes an important factor to influence N in addition to the hot carrier energy E_0. Therefore, $P(E)$ is determined by either P_{i} or P_{ii} according to the value of N. With $P(E)$ calculated, IQE in regions I and II can be easily obtained through equation (2).

However, $P(E)$ in equations (3.1) and (3.2) cannot be applied directly for the Au film in region III shown in figure 1(b), where there is only one point in direct contact with Si. The momentum of a hot carrier in this region can be orthogonally decomposed into two components either along the horizontal direction or the vertical direction. This is illustrated as two emission cones along the x and y directions in figures 2(c) and (d), respectively. The emission solid angle, Ω, is determined by $k \cdot \cos\Omega = k_{\mathrm{SB}}$ as shown in figure 2(b). Limited by the same thickness of the Au film both horizontally and vertically, the horizontal and vertical emission probabilities are equal and both determined by $P(E)$ expressed in equations (3.1) and (3.2). Since only half of the emission cone lies in region III, a hot carrier in each cone is only half as likely to undergo emission, that is, $P_{\mathrm{h}}(E) = P_{\mathrm{v}}(E) = P_{\mathrm{i}}/2$ when $N = 0$ and $P_{\mathrm{h}}(E) = P_{\mathrm{v}}(E) = P_{\mathrm{ii}}/2$ when $N > 0$. Therefore, this corner is symmetrical. If these two cones are separated with the solid angle smaller than $\pi/4$, i.e. $\Omega < \pi/4$, as shown in figure 2(c), the total IPE probability will be defined by the sum of the probabilities of each half cone divided by 2 (the denominator of 2 is mainly due to the fact that the hot carrier can be emitted only in one of the emission cones, i.e., either the horizontal or the vertical), that is,

$$P(E) = \frac{P_{\mathrm{h}}(E) + P_{\mathrm{v}}(E)}{2} = \begin{cases} P_{\mathrm{i}}/2, & \text{when } N = 0; \\ P_{\mathrm{ii}}/2, & \text{when } N > 0. \end{cases} \quad (4)$$

On the other hand, if $\Omega \geqslant \pi/4$, the two emission cones overlap as shown in figure 2(d). The overlapping angle θ is equal to (2Ω-$\pi/2$). Then, the total IPE probability is the sum of the probabilities for the two half emission cones minus the overlapping probability P_{o} and finally divided by 2 (the reason for the denominator of 2 is the same as that for equation (4)), that is,

$$P(E) = \frac{P_{\mathrm{h}}(E) + P_{\mathrm{v}}(E) - P_o}{2} = \begin{cases} \left(P_{\mathrm{i}} - P_{\mathrm{i}}|_{\theta/2}\right)/2, & \text{when } N = 0; \\ \left(P_{\mathrm{ii}} - P_{\mathrm{ii}}|_{\theta/2}\right)/2, & \text{when } N > 0. \end{cases} \quad (5)$$

Based on equations (4) and (5), the IQE in region III can be easily obtained using equation (2) and are plotted in figures 3(c) and (d) for p-Si and n-Si based Au-Si symmetrical corners, respectively. For the cases based on n-Si, $\Omega < \pi/4$ holds in the whole wavelength range due to the high Schottky

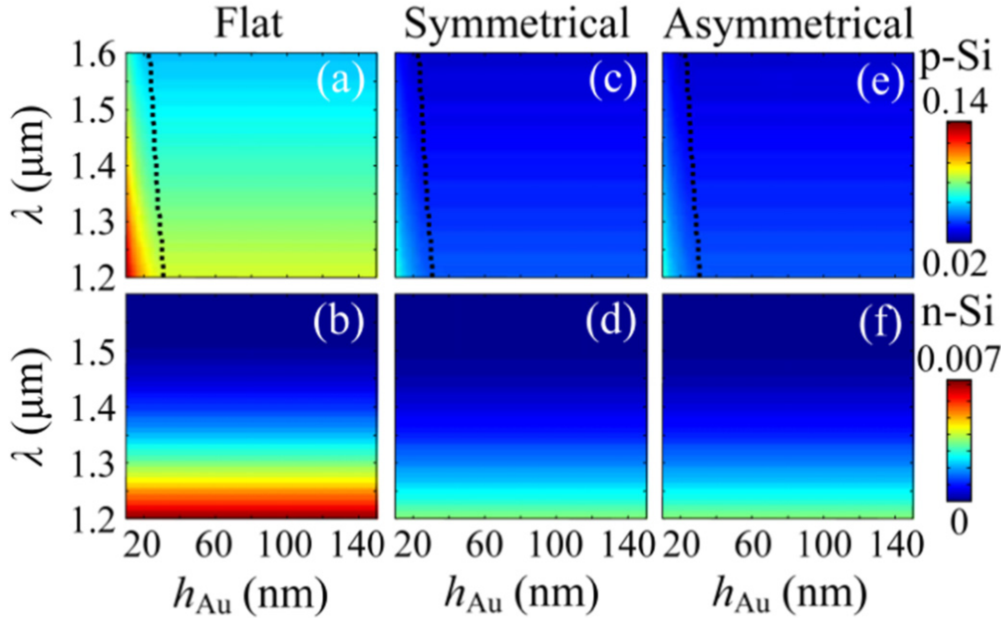

Figure 3. IQE as a function of the Au electrode thickness h_{Au} and the incident photon wavelength λ for (a), (b) flat Au–Si contacts, (c), (d) symmetrical corners, and (e), (f) asymmetrical corners based on p-Si (top) and n-Si (bottom). The black dotted curves in figures 3(a), (c) and (e) indicate where IQE becomes independent of h_{Au}.

barrier ($\Phi_B = 0.8$ eV) and it leads to just half of the values for the flat Au–Si contact shown in figure 3(d). For p-Si based symmetrical corner, IQE follows the same trend as that shown in figure 3(a) for the flat contact. The turning point of h_{Au} remains the same for all the input wavelengths, as denoted by the black dotted line in figure 3(c). Compared with the values shown in figure 3(a), the IQE at each point falls to about half, meaning that the overlap of the emission cones, shown in figure 2(d), contributes little to the total IPE probability.

For the structure with $h_{SU8} = 200$ nm shown in figure 1(c), the Au film apparently consists of two parts. One is region II, covering the top of the Si ridge, where $P(E)$ can be easily calculated by equations (3.1) and (3.2).The other is different from regions I to III and is named region IV. Like region III, there is also only one point directly touching Si and the emission probability can also be depicted by two orthogonal emission cones as shown in figures 2(e) and (f). But differently, the Au film is very thick in the horizontal direction (too thick to allow a second emission of the hot carriers transporting horizontally), while the vertical thickness varies. Therefore, $P_h(E) = P_i/2$ is not always equal to $P_v(E) = P_{ii}/2$ and region IV can be regarded asymmetrical. When $\Omega < \pi/4$, the two emission cones do not overlap as shown in figure 2(e). $P(E)$ can be calculated as follows (the same reason for the denominator of 2 with that for equation (4)):

$$P(E) = \left[P_h(E) + P_v(E)\right]/2 = \left(P_i + P_{ii}\right)/4. \tag{6}$$

When $\Omega \geqslant \pi/4$ as shown in figure 2(f), the emission cones overlap. Different from region III, it is difficult to calculate P_o due to the asymmetry. Here, we simply assume that all the hot carriers in the overlapping region have 50% emission probability from the vertical cone and 50% from the horizontal cone. Then, we get $P(E)$ as follows:

$$\begin{aligned} P(E) &= \left[P_h(E) + P_v(E) - P_o\right]/2 \\ &= \left(P_i + P_{ii} - P_i|_{\theta/2} - P_{ii}|_{\theta/2}\right)/4. \end{aligned} \tag{7}$$

If $N = 0$ holds for the vertical emission, $P_v = P_{ii}/2$ is reduced to $P_i/2$ and becomes equal to P_h. As a result, $P(E)$ and thus IQE in region IV can be treated as in region III with $N = 0$. From figures 3(e) and (f), one can see that the values of IQE for both p-Si and n-Si cases are very close to those of their symmetrical counterparts. From figure 3(e) for the p-Si based asymmetrical corner, the effect of h_{Au} on IQE is also observed, which is indicated by the black dotted curve. So far, the IQE for both diode structures shown in figures 1(b) and (c) can be obtained by the above model.

Like IQE, the absorption, A, also differs for different regions and it can be calculated based on the finite-difference time domain method (Lumerical FDTD Solutions). The fundamental TE or TM mode of the dielectric Si ridge waveguide is set as the input. Three-dimensional monitors are set to record the electric field intensity distribution ($|E|^2$) of different parts of the Au film. The absorption can be obtained as follows:

$$A = \frac{\iiint \frac{\pi c}{\lambda} \cdot \mathrm{Im}(\varepsilon)|E|^2 \mathrm{d}x\mathrm{d}y\mathrm{d}z}{\text{source power}}, \tag{8}$$

where $\mathrm{Im}(\varepsilon)$ is the imaginary part of the dielectric constant of Au, and c is the speed of light in vacuum. To calculate the total responsivities of the photodetectors shown in figures 1(b) and (c), we extended equation (1) as the sum of the responsivities in the compositional regions expressed in equations (9) and (10) below for our photodetector and the

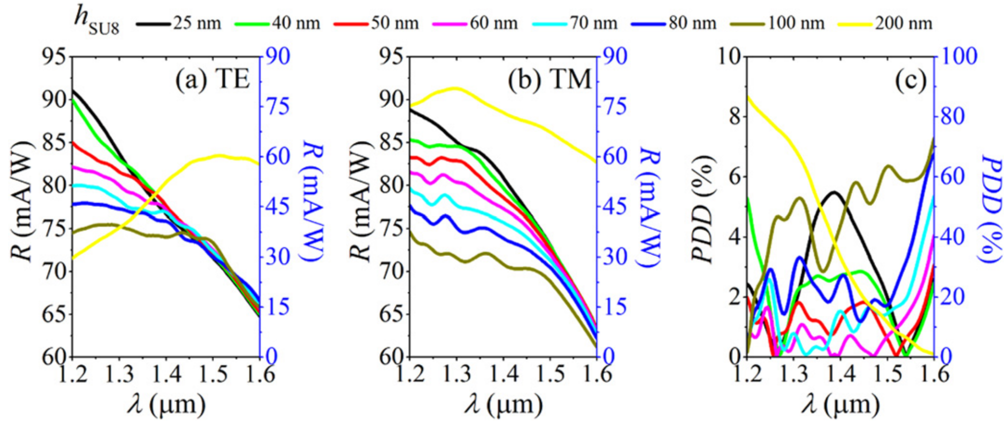

Figure 4. Responsivity, R, varies with the SU8 film thickness, h_{SU8}, for (a) TE and (b) TM polarizations. (c) Polarization dependent deviations of responsivity, PDD. $h_{SU8} = 25, 40, 50, 60, 70, 80, 100, 200$ nm are considered and the Au film thickness is fixed as $h_{Au} = 20$ nm. In all the three figures, the comparative curves representing the case of $h_{SU8} = 200$ nm (i.e. the comparative case of figure 1(c)) are all calibrated by the right vertical axes to give clear comparison.

comparative device, respectively:

$$R = \frac{q}{E_0} \cdot \left(A_{\mathrm{I}} \cdot \mathrm{IQE}_{\mathrm{I}} + A_{\mathrm{II}} \cdot \mathrm{IQE}_{\mathrm{II}} + A_{\mathrm{III}} \cdot \mathrm{IQE}_{\mathrm{III}}\right), \quad (9)$$

$$R = \frac{q}{E_0} \cdot \left(A_{\mathrm{II}} \cdot \mathrm{IQE}_{\mathrm{II}} + A_{\mathrm{IV}} \cdot \mathrm{IQE}_{\mathrm{IV}}\right), \quad (10)$$

where, $A_x \cdot \mathrm{IQE}_x$ is the external quantum efficiency in region x. Equations (9) and (10) mean that the photocurrent collected by the electrode is contributed by all the hot carriers emitted from all the compositional regions: regions I–III in figure 1(b) and regions II and IV in figure 1(c).

For a PD, dark current is also a very important parameter, which determines the sensitivity or the smallest detectable power of a PD. For a Schottky diode, the dark current can be calculated using equation (11) given below [19]:

$$I_{\mathrm{dark}} = C_{\mathrm{area}} A^{**} T^2 \mathrm{e}^{-(q\Phi_{\mathrm{B}}/k_{\mathrm{B}}T)}, \quad (11)$$

where C_{area} is the Schottky contact area, A^{**} is the effective Richardson constant, equal to 112 and 32 $\mathrm{A cm^{-2} K^{-2}}$ for electrons and holes, respectively [26], k_{B} is the Boltzmann constant and $T = 300$ K at room temperature.

3. Results and discussion

In the following, only the p-Si based Schottky diode (instead of n-Si based one) is considered because it has much higher IQE, as shown in figure 3, and is, therefore, promising to produce a much larger photocurrent with the same diode structure. Since h_{SU8} plays a very important role in tuning the sidewall coverage of Au and further tuning the absorption polarization dependence, we first investigated the responsivity, R, of the photodector as a function of h_{SU8}. The curves representing R at $h_{SU8} = 25, 40, 50, 60, 70, 80, 100$ and 200 nm are plotted in figures 4(a) and (b) for both TE and TM polarizations, respectively. From these two figures, it is seen that with the Au film covering part of the sidewalls of the Si ridge waveguide (i.e. $h_{SU8} < 200$ nm as schematically shown in figure 1(b)), R becomes much higher than that for the case of $h_{SU8} = 200$ nm (i.e. no sidewall coverage of Au, as schematically shown in figure 1(c)). For TE polarization, when $h_{SU8} < 70$ nm, R decreases nearly linearly as the wavelength increases in the whole wavelength range of 1.2–1.6 μm, as shown in figure 4(a). As h_{SU8} increases to 100 nm, the R spectrum in the short wavelength range below about 1.5 μm becomes lower and flatter, while in the long wavelength range, R behaves similarly for all values of h_{SU8} considered here and drops quickly as λ increases. For TM polarization, the R spectrum falls gradually when h_{SU8} increases to 100 nm as shown in figure 4(b). Interference ripples are observed in the short wavelength range. To quantitatively characterize the polarization sensitivity, we define the polarization dependent deviations (PDD), of the responsivity between TE and TM polarizations as follows,

$$\mathrm{PDD} = \frac{|R_{\mathrm{TE}} - R_{\mathrm{TM}}|}{\left(R_{\mathrm{TE}} + R_{\mathrm{TM}}\right)/2} \times 100\%. \quad (12)$$

Based on figures 4(a) and (b), PDD is calculated according to equation (12) and plotted in figure 4(c) for different values of h_{SU8}. It is shown that the PDD spectrum for the case of $h_{SU8} = 50$ nm is the lowest (below 3%) in the whole wavelength range of interest. The case of $h_{SU8} = 60$ nm shows better polarization control in the considered wavelength range except $\lambda > 1.55$ μm. As h_{SU8} decreases or increases, higher polarization sensitivities appear. PDD approaches a maximum in the short wavelength range when $h_{SU8} = 200$ nm (the comparative case with no coverage of Au on the sidewall of the Si ridge waveguide). This indicates that a certain degree of coverage of the Au film on the sidewall of the Si ridge waveguide is beneficial to minimizing the polarization sensitivity of the responsivity.

In order to have a more fundamental understanding of the polarization tuning, the total absorption, reflection, and transmission spectra of two typical cases of $h_{SU8} = 50$ and 200 nm are investigated, as demonstrated in figure 5. From the total absorption spectra shown in figure 5(a), it is seen that for the comparative detector of $h_{SU8} = 200$ nm, the

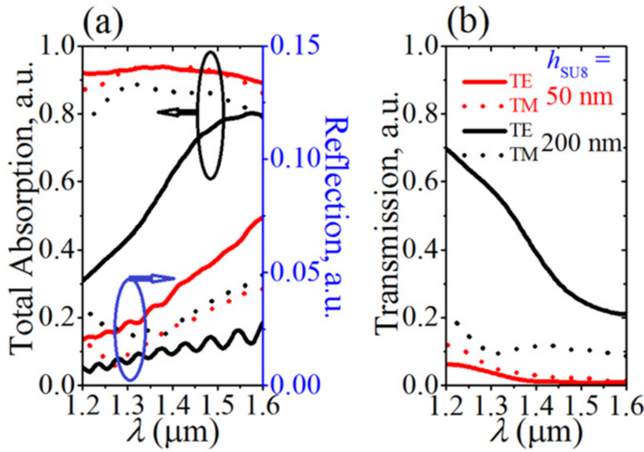

Figure 5. Comparisons of Schottky diodes of $h_{SU8} = 50$ (red) and 200 nm (black) for TE (solid curves) and TM (dotted curves) polarizations on (a) total absorption and reflection (which is calibrated by the right vertical axis); and (b) transmission. The Au film thickness is $h_{Au} = 20$ nm.

absorption for TE polarization is lower than that for TM polarization. Both of them are much lower than those of our detector with $h_{SU8} = 50$ nm, whose total absorption is greater than about 85% for both polarizations with apparently a very weak polarization deviation in the whole wavelength range. This indicates that the sidewall coverage of Au substantially enhances the total absorption, especially for TE polarization, leaving little light passing through the Au Schottky contact region of only 4 μm in length as shown in figure 5(b). It is noted that the absorption cannot be increased even more by simply increasing the length of the Schottky contact region due to the reflection induced by the mode mismatch between the input Si ridge waveguide and the Au covered Si ridge waveguide (i.e. the Schottky contact region), as shown in figure 5(a).

To show how the polarization sensitivity is eliminated effectively, we investigated the fundamental mode variations at a typical wavelength of, e.g. $\lambda = 1.4$ μm in the center of the considered wavelength range, for the Si ridge waveguides with and without Au coverage when $h_{SU8} = 50$ and 200 nm and the results are plotted in figure 6. Here the finite-difference method (embedded in Lumerical FDTD Solutions) is employed, which is much simpler in comparison with the FDTD method by doing only two-dimensional cross-sectional calculations and thereby has been widely applied to the calculations and analyses of the mode distributions for any waveguide structures. When $h_{SU8} = 50$ nm, being excited by the fundamental modes in the front Si ridge waveguide shown in figures 6(a)–(d), the fundamental modes of the connecting Au covered Si ridge waveguide are excited, where the electric field is mainly concentrated along the Au–Si interfaces horizontally for the quasi-TE mode and vertically for the quasi-TM mode, as shown in figures 6(e)–(h). The field coverage over the Au leads to great absorption in it for both TE and TM polarizations according to equation (8) as shown in figure 5(a). When $h_{SU8} = 200$ nm, the horizontal confinement of the Si ridge waveguide is mainly induced by the thick SU8 film due to its lower refractive index versus that of the central Si. Therefore, the fundamental TE mode is not influenced much by the top Au thin film for the Au covered Si ridge waveguide, as shown in figure 6(m), in comparison with that in figure 6(i). The electric field is still mainly confined in the high-index Si and only a little light is coupled into Au and absorbed there. Thus, low absorption and high transmission appear for TE polarization as shown in figure 5. For TM polarization, the electric field is dominated by the y-component, as shown in figure 6(l), and $|E_y|$ becomes tightly confined at the top Au–Si interface when the Au thin film is deposited as shown in figure 6(p). In this case, high absorption and low transmission is predicted as shown in figure 5. This shows remarkable polarization-dependent absorption for the case of $h_{SU8} = 200$ nm. From figure 6, one can see clearly how the polarization-dependent absorption in figure 5 and thus the responsivity in figure 4 are minimized by simply reducing the thickness of the SU8 film and covering the sidewalls of the Si ridge waveguide with Au.

For both cases of $h_{SU8} = 50$ and 200 nm, when $\lambda > 1.4$ μm, both dielectric and plasmonic modes are tightly confined (not shown here), leading to larger mode mismatch and consequently larger reflection loss, as shown in figure 5(a). On the other hand, when $\lambda < 1.4$ μm, the modes are loosely confined (not shown either), and the input fundamental mode in the Si ridge waveguide can be easily coupled to the modes in the Schottky contact region. That is why a smaller reflection loss but a larger transmission loss appear in figure 5, especially for the TE polarization. Therefore, the absorption of our Schottky diode (red curves in figure 5(a)) is higher in the middle wavelength range than in the ranges beyond it.

Another important parameter is the Au film thickness, which influences not only the IQE (shown in figure 3) but also the light absorption of our Schottky photodetector. Here, we fix $h_{SU8} = 50$ nm (with which PDD can be minimized the most significantly when $h_{Au} = 20$ nm as shown in figure 4) and investigate the effect of h_{Au} on the total absorption and responsivity of our detector and the polarization dependence of the responsivity. Figure 7(a) shows the total absorption spectra of our photodetectors with $h_{Au} = 10$, 20, 30, 50, 70, 90, and 150 nm, respectively. When $h_{Au} \geqslant 50$ nm, the absorption spectrum tends not to change much with increasing h_{Au} for both TE and TM polarizations. This is mainly due to the strong optical field tightly confined at the Au–Si interfaces that can be sufficiently absorbed with a 50 nm thick Au film. An even thicker Au film will not significantly increase the light absorption within it. Consequently, R in figure 7(b) and PDD in figure 7(c) do not show any significant change with h_{Au} either (also due to the unchanged IQE shown in figure 3). However, PDD is very large in the whole wavelength range for $h_{Au} \geqslant 50$ nm. As h_{Au} decreases, PDD decreases first and then quickly increases as shown in figure 7(c). At $h_{Au} = 20$ nm, the PDD spectrum reaches the lowest level in the whole wavelength range from 1.2 to 1.6 μm. Due to the linearly decreasing IQE as λ in each part of the Au film, as shown in figure 3, the spectral features appearing in the absorption spectra in figure 7(a) become

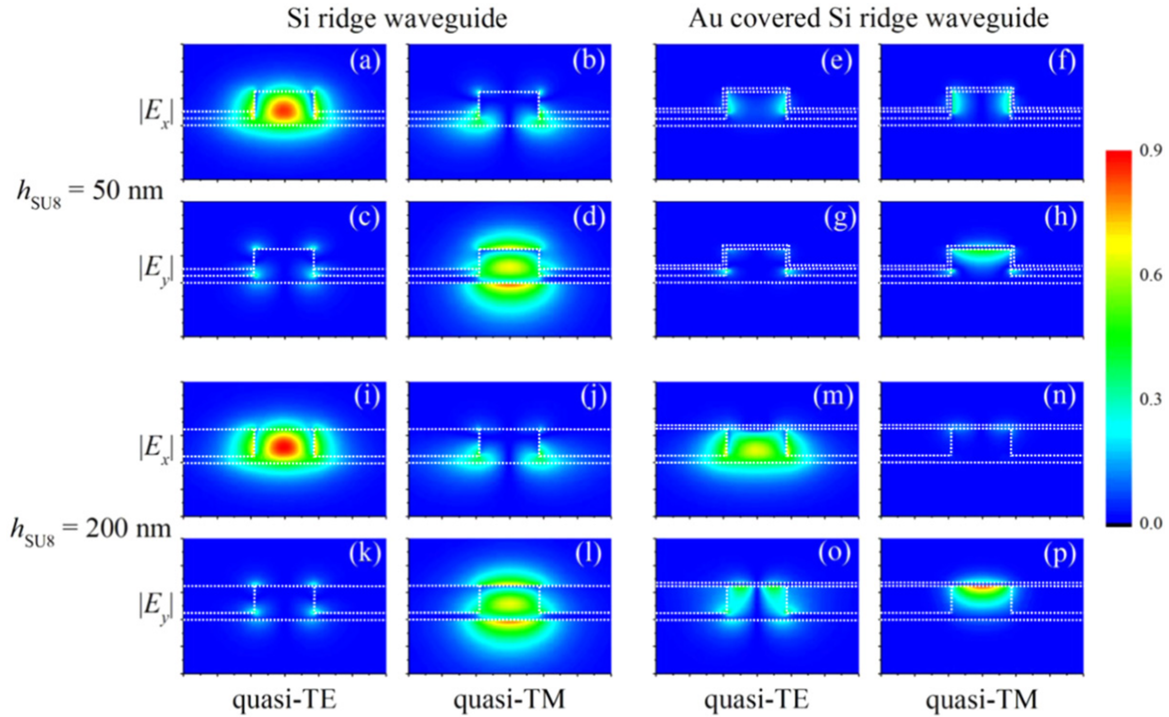

Figure 6. Fundamental mode distributions at $\lambda = 1.4\ \mu$m of Si ridge waveguide (left) and Au covered Si ridge waveguide (right) when $h_{\mathrm{SU8}} = 50$ nm (top) and 200 nm (bottom). The waveguide structures are indicated by the white dotted lines. The Au film thickness is $h_{\mathrm{Au}} = 20$ nm.

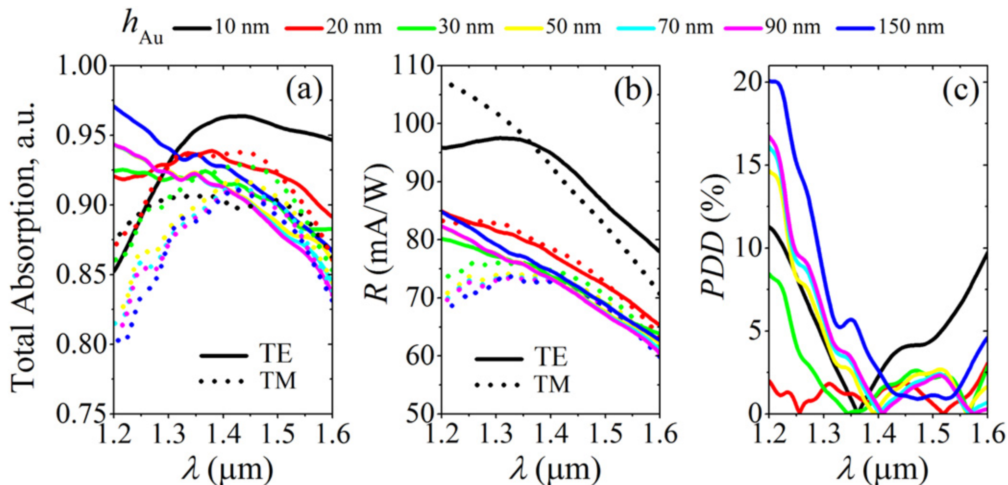

Figure 7. (a) Total absorption, (b) responsivity, R, for TE (solid curves) and TM (dotted curves) polarizations, and (c) polarization dependent deviation, PDD, of responsivity, for our Schottky photodetectors with $h_{\mathrm{Au}} = 10$, 20, 30, 50, 70, 90 nm, and 150 nm. The SU8 film thickness is $h_{\mathrm{SU8}} = 50$ nm.

greatly weakened in the responsivity spectra as shown in figure 7(b) for both TE and TM polarizations. At $h_{\mathrm{Au}} = 10$ nm, the IQE is the highest in each part of the Au film among all the cases with values of h_{Au} considered here. Therefore, the responsivity spectrum rises to the highest level, especially in the short wavelength range, even though the absorption spectrum lies in the same range as the other cases with larger h_{Au}. In this case, the IQE dominates the responsivity spectrum. But PDD is too large in the whole wavelength range in comparison with that for $h_{\mathrm{Au}} = 20$ nm.

From the above analysis, we find that, when $h_{\mathrm{SU8}} = 50$ nm and $h_{\mathrm{Au}} = 20$ nm, our Schottky diode has the lowest PDD over a wide wavelength range from 1.2 to 1.6 μm as shown in figures 4(c) and 7(c). For this diode, over 85% of the input light is absorbed by an only 4 μm long Au film, which is much smaller than those reported in [11, 12]. Because of this, its dark current calculated by equation (11) is very low, i.e., $I_{\mathrm{dark}} = 0.145\ \mu$A, smaller than those reported in [11, 12]. Figure 8 shows that the photocurrent generated by 1 W of the incident light is about 5 orders of magnitude larger

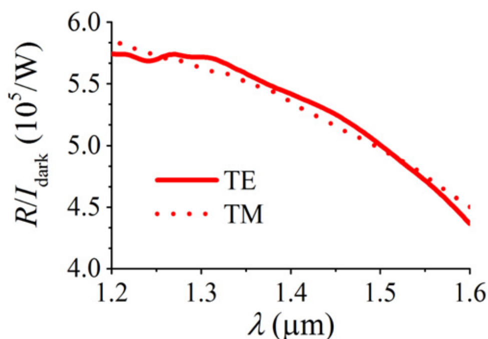

Figure 8. The ratio of the responsivity to the dark current as a function of the light wavelength for both TE (solid curve) and TM (dotted curve) polarizations for our Schottky photodetectors with $h_{\text{Au}} = 20$ nm, and $h_{\text{SU8}} = 50$ nm.

than the dark current, meaning superior detection ability of our Schottky diode.

4. Conclusion

In summary and conclusion, we have proposed a broadband, polarization-insensitive and high-efficiency hot-carrier Schottky diode integrated with a plasmonic Si ridge waveguide for detection of photons in the optical communication wavelength range of 1.2–1.6 μm. A systematic analysis of the performance characteristics using the extensive physical model leads to the conclusion that the polarization sensitivity can be greatly minimized (PDD $< 3\%$) by our photodetector with $h_{\text{SU8}} = 50$ nm and $h_{\text{Au}} = 20$ nm (figure 1(b)) in the wavelength range under study. It has much higher responsivity than the one with the same Schottky contact length but only with top coverage of Au (figure 1(c)). All of these excellent properties are attributed to the plasmonic modes excited within the highly-absorptive plasmonic waveguide with top and sidewall coverage of Au, which can be easily tuned by reducing or increasing the thickness of the SU8 insulator layer. Because of the short length, its dark current is also very low, i.e. $I_{\text{dark}} = 0.145$ μA, much smaller than those reported in [11, 12]. These results collectively suggest that our design is highly promising for applications in high-density silicon photonic integration. We expect to have it realized experimentally in the near future.

Acknowledgments

This work was supported by the National Natural Science Foundation of China (Nos. 61307078, 91233208, 91233119, and 11174250), the National High Technology Research and Development Program (863) of China (No. 2012AA030402), the Specialized Research Fund for the Doctoral Program of Higher Education (No. 20130101120134), and the Fundamental Research Funds for the Central Universities (No. 2014QNA5018). L Yang also acknowledges the financial support from China Scholarship Council.

References

[1] Sze S M and Ng K K 2006 *Physics of Semiconductor Devices* (New York: Wiley)
[2] Knight M W, Sobhani H, Nordlander P and Halas N J 2011 Photodetection with active optical antennas *Science* **332** 702–4
[3] Sobhani A, Knight M W, Wang Y, Zheng B, King N S, Brown L V, Fang Z, Nordlander P and Halas N J 2013 Narrowband photodetection in the near-infrared with a plasmon-induced hot electron device *Nat. Commun.* **4** 1643
[4] Alavirad M, Mousavi S S, Roy L and Berini P 2013 Schottky-contact plasmonic dipole rectenna concept for biosensing *Opt. Express* **21** 4328–47
[5] Tian Y and Tatsuma T 2005 Mechanisms and applications of plasmon-induced charge separation at TiO_2 films loaded with gold nanoparticles *J. Am. Chem. Soc.* **127** 7632–7
[6] Reineck P, Lee G P, Brick D, Karg M, Mulvaney P and Bach U 2012 A solid-state plasmonic solar cell via metal nanoparticle self-assembly *Adv. Mater.* **24** 4750–5
[7] Pelayo García de Arquer F, Mihi A, Kufer D and Konstantatos G 2013 Photoelectric energy conversion of plasmon-generated hot carriers in metal–insulator–semiconductor structures *ACS Nano* **7** 3581–8
[8] Casalino M, Sirleto L, Iodice M, Saffioti N, Gioffrè M, Rendina I and Coppola G 2010 Gu/p-Si schottky barrier-based near infrared photodetector integrated with a silicon-on-insulator waveguide *Appl. Phys. Lett.* **96** 241112
[9] Zhu S, Yu M B, Lo G Q and Kwong D L 2008 Near-infrared waveguide-based nickel silicide Schottky-barrier photodetector for optical communications *Appl. Phys. Lett.* **92** 081103
[10] Zhu S, Lo G Q and Kwong D L 2011 Theoretical investigation of silicide schottky barrier detector integrated in horizontal metal–insulator–silicon–insulator–metal nanoplasmonic slot waveguide *Opt. Express* **19** 15843–54
[11] Akbari A and Berini P 2009 Schottky contact surface-plasmon detector integrated with an asymmetric metal strip waveguide *Appl. Phys. Lett.* **95** 021104
[12] Scales C, Breukelaar I and Berini P 2010 Surface-plasmon schottky contact detector based on a symmetric metal strip in silicon *Opt. Lett.* **35** 529–31
[13] Goykhman I, Desiatov B, Khurgin J, Shappir J and Levy U 2011 Locally oxidized silicon surface-plasmon schottky detector for telecom regime *Nano Lett.* **11** 2219–24
[14] Goykhman I, Desiatov B, Khurgin J, Shappir J and Levy U 2012 Waveguide based compact silicon schottky photodetector with enhanced responsivity in the telecom spectral band *Opt. Express* **20** 28594–602
[15] Liang D, Fang A W, Chen H, Sysak M N, Koch B R, Lively W, Raday O, Kuo Y, Jones R and Bowers J E 2009 Hybrid silicon evanescent approach to optical interconnects *Appl. Phys.* A **95** 1045–57
[16] Carey J E, Crouch C H, Shen M and Mazur E 2005 Visible and near-infrared responsivity of femtosecond-laser microstructured silicon photodiodes *Opt. Lett.* **30** 1773–5
[17] Liu Y, Chow C W, Cheung W Y and Tsang H K 2006 In-line channel power monitor based on helium ion implantation in silicon-on-insulator waveguides *IEEE Photonics Technol. Lett.* **18** 1882–4
[18] Liang T K, Tsang H K, Day I E, Drake J, Knights A P and Asghari M 2002 Silicon waveguide two-photon absorption detector at 1.5 μm wavelength for autocorrelation measurements *Appl. Phys. Lett.* **81** 1323–5
[19] Scales C and Berini P 2010 Thin-film schottky barrier photodetector models *IEEE J. Quantum Electron.* **46** 633–43
[20] Maier S A 2007 *Plasmonics: Fundamentals and Applications* (Berlin: Springer)

[21] Fang Z, Liu Z, Wang Y, Ajayan P M, Nordlander P and Halas N J 2012 Graphene–antenna sandwich photodetector *Nano Lett.* **12** 3808–13
[22] Fang Z, Wang Y, Liu Z, Schlather A, Ajayan P M, Koppens F H L, Nordlander P and Halas N J 2012 Plasmon-induced doping of graphene *ACS Nano* **6** 10222–8
[23] Stuart R N, Wooten F and Spicer W E 1963 Mean free path of hot electrons and holes in metals *Phys. Rev. Lett.* **10** 7–9
[24] Schluter M 1982 Theoretical models of schottky barriers *Thin Solid Films* **93** 3–19
[25] Cowley A M and Sze S M 1965 Surface states and barrier height of metal–semiconductor systems *J. Appl. Phys.* **36** 3212–20
[26] Kramer P and van Ruyven L J 1972 Position of the band edges of silicon under uniaxial stress *Appl. Phys. Lett.* **20** 420–2